




High-Frequency Ground Motion and Source Characteristics of the 2008 Wenchuan and 2013 Lushan, China, Earthquakes

LINGYUAN MENG,^{1,2}  YANG ZANG,^{1,3} A. MCGARR,² and LONGQUAN ZHOU¹

Abstract—The 2008 $M_W7.9$ Wenchuan and the 2013 $M_W6.6$ Lushan earthquakes, which both occurred on the Longmen Shan thrust belt, show some interesting similarities and differences. Whereas the Wenchuan earthquake entailed a rupture zone that extended about 300 km northeastward, with fault slip extending to the surface, the Lushan earthquake was the result of a buried and much more compact zone of rupture. The high-frequency ground motions, however, for these two earthquakes, as measured by the peak ground acceleration, were evidently influenced by neither the extent of rupture nor the presence or absence of surface rupture. The source parameters for these two earthquakes tend to confirm the idea that high-frequency ground motion is controlled by stress changes in the rupture zone that give rise to the radiated ground acceleration. The apparent stresses for the Wenchuan and Lushan earthquakes are about 0.5 and 0.75 MPa, respectively, and the stress drops, in the same order, are about 2.5 and 3.5 MPa. The ratios of average stress drop to apparent stress are in the range 4.5–5 for both events, consistent with expectations based on the Brune (J Geophys Res 75(26):4997–5009, 1970) source model.

Key words: 2008 Wenchuan earthquake, 2013 Lushan earthquake, stress drop, near-fault ground motion, NGA-West2, EXSIM.

1. Introduction

The 12 May 2008 $M_W7.9$ Wenchuan earthquake ruptured the Longmen Shan thrust belt, which separates the Tibetan Plateau from the Sichuan Basin. The rupture, thrust faulting with a right-lateral strike-slip component, propagated unilaterally northeastward for approximately 300 km from its epicenter (Chen et al. 2008). The highly destructive Wenchuan earthquake,

felt throughout the Sichuan, Shanxi and Gansu provinces, was well recorded at nearly 100 strong-motion stations within 300 km of the rupture zone (Li et al. 2008; Wang et al. 2010; Wang and Lu 2011).

The 20 April 2013 $M_W6.6$ Lushan earthquake, also destructive, occurred on the same thrust belt, and was located about 80 km south-southwest of the epicenter of the Wenchuan earthquake. Analysis of local and teleseismic data indicate that the Lushan earthquake initiated at a depth of 13 km, with a reverse-faulting source mechanism (Han et al. 2014). In contrast to the Wenchuan earthquake, the Lushan event ruptured a blind thrust fault (Xu et al. 2013; Zhang et al. 2013). Its largest peak ground acceleration (PGA) of 1005.4 cm/s^2 was observed on the east–west component at the Baoxing Station (51BXD), the first observation in this region of a horizontal PGA exceeding 1 g (Wen and Ren 2014).

The Longmen Shan thrust belt coincides with steep gradients in crustal thickness, from about 60 km to the west to about 40 km to the east. This thrust belt is under horizontal compression from the eastward extrusion of the Tibetan Plateau against the more rigid Sichuan Basin in the western part of the Yangtze craton (Wang et al. 2007; Xu et al. 2009).

Whereas the Wenchuan earthquake ruptured unilaterally toward the northeast, the Lushan earthquake rupture appears to have been bilateral and much more compact. The distributions of aftershocks for the two earthquakes are separated by a gap of about 60 km (Chen et al. 2013). In response to the deadly Wenchuan earthquake, there was a significant increase in the density of broadband and strong-motion stations throughout southwestern Sichuan province, including the vicinity of the 2013 Lushan earthquake (Mooney and Wang 2014). These data have been used in

¹ China Earthquake Networks Center (CENC), Beijing 100045, China. E-mail: meng.lingyuan@hotmail.com

² U. S. Geological Survey (USGS), Earthquake Science Center, Menlo Park, CA 94025, USA.

³ Institute of Geophysics, China Earthquake Administration, Beijing 100081, China.

numerous studies of source parameters, wave propagation, and site effects in the Sichuan region of China (e.g., Wang et al. 2018; Wen et al. 2018; Ren et al. 2018). The finite fault model for the Wenchuan earthquake (Chen et al. 2008) shows a maximum slip of 6 m within a rupture zone dipping steeply southwestward and extending about 300 km along the strike. Unilateral rupture propagation toward the northeast resulted in considerable directivity in contrast to the Lushan earthquake for which the bilateral rupture resulted in little or no directivity.

The primary source parameters are given by the earthquake catalogs from the China Earthquake Networks Center (CENC, see Data and Resources) and Global Centroid Moment Tensor project (GCMT, see Data and Resources), including the United States Geological Survey (USGS, see Data and Resources) Energy and Broadband Solution. For the Wenchuan event, the seismic moment $M_0 = 8.97 \times 10^{20} \text{ N} \cdot \text{m}$, the radiated energy $E_S = (1.4 \sim 1.6) \times 10^{16} \text{ N} \cdot \text{m}$, and the apparent stress τ_a^{WC} is about $0.47 \sim 0.54 \text{ MPa}$, as estimated using

$$\tau_a = \mu E_S / M_0, \quad (1)$$

(Wyss and Brune, 1968) where the rigidity modulus $\mu = 3.0 \times 10^4 \text{ MPa}$.

The Lushan earthquake, located along the same fault zone between the western Sichuan Basin and the eastern Tibetan Plateau, had an almost pure thrust mechanism. The finite-fault slip model (Chen et al. 2013) showed an up-dip rupture dimension of 20–30 km on a fault of length 40 km along the strike. Maximum slip was estimated to be about 1.6 m near the hypocentral depth, and rupture speed was also about 3.0 km/s (Chen et al. 2013). The radiated seismic energy was estimated as $E_S = (2.3 \sim 2.8) \times 10^{14} \text{ J}$, based on the USGS Energy and Broadband Solution, and the seismic moment $M_0 = 1.02 \times 10^{19} \text{ N} \cdot \text{m}$, based on the GCMT (see Data and Resources). Accordingly, τ_a^{LS} is about $0.68 \sim 0.82 \text{ MPa}$ from Eq. (1). Thus, the apparent stress for the Lushan earthquake appears to be slightly greater than for the Wenchuan earthquake.

Our intent here is to investigate the high-frequency ground motions from the Wenchuan and Lushan earthquakes to address several issues,

including: (1) the relationships between the source parameters and the high-frequency ground motion, especially in the environs of the rupture zones, (2) the extent to which the ground-motion prediction equations from NGA-West2 accord with observations of high-frequency ground motion for these two earthquakes, and (3) whether the high-frequency ground motion depends in any discernable way on the existence, or otherwise, of surface rupture (Xu et al. 2009, 2013; Zhang et al. 2013; Wang et al. 2008).

2. Observations of Ground Motion

During the Wenchuan earthquake, the National Strong Motion Observation Network System (NSMONS) collected a large number of ground-motion recordings from the mainshock. For the Wenchuan mainshock, 460 accelerometers were triggered, yielding almost 1400 components of acceleration. Among them, more than 100 components exceed 100 cm/s^2 , and 7 are larger than 600 cm/s^2 . The largest peak ground acceleration (PGA) was recorded at Wolong station in Wenchuan County (51WCW) which is located on the hanging wall, close to the surface rupture. The PGAs recorded in the EW, NS, and UD directions are 957.7, 655.8, and 948.1 cm/s^2 , respectively. The record with the second largest peak acceleration was obtained at Qingping station in Mianzhu (51MZQ), where the peak accelerations recorded in the EW, NS, and vertical directions are 824.1, 802.5, and 622.9 cm/s^2 , respectively. Station 51MZQ is about 88 km from the epicenter and roughly 1 km from the middle of the fault trace on the footwall (Li et al. 2008; Wang et al. 2010; Wang and Lu 2011).

For the Lushan event, 121 digital ground-motion accelerometers of NSMONS were triggered, recording more than 350 components with PGA values larger than 10 cm/s^2 . The largest PGA was observed at station 51BXD in Baoxing County, which recorded PGAs in the EW, NS, and UD directions of 1005.4, 823.5, and 478.0 cm/s^2 , respectively. The second largest horizontal recording was obtained at station 51BXZ in Baoxing County, with PGAs in EW, NS, and UD directions of 583.4, 316.2, and 387.2 cm/s^2 , respectively. A total of 79 accelerometers that

recorded mainshock ground motion are within 100 km of the rupture, including 13 located within 20 km of the epicenter, making the Lushan earthquake an exceptionally well-recorded blind reverse-fault event (Wen and Ren 2014). The substantial ground-motion data sets of the Wenchuan and Lushan earthquakes (Figs. 1, 2) provided a good opportunity to study the characteristics of strong motions for large intraplate earthquakes (Mooney and Wang 2014).

2.1. Near-Fault Strong Ground Motion

Two distance measures, commonly used in the analyses of strong ground motion are R_{rup} , the

shortest distance between the station and the rupture surface, and R_{JB} , or Joyner–Boore distance, as the closest horizontal distance from the station to the surface projection of the rupture surface (Boore et al. 2014). We have used R_{JB} as the distance metric because it was most straightforward to use the epicenters of well-relocated aftershocks to determine the surface projections of the ruptures for both earthquakes (Wang et al. 2008, 2010; Han et al. 2014; Ren et al. 2018).

To investigate near-fault ground motion, we have considered data recorded at $R_{JB} \leq 10$ km (Table 1, Figs. 3 and 4). For the Wenchuan event, there are 45 stations located in the region with $R_{JB} < 100$ km, and

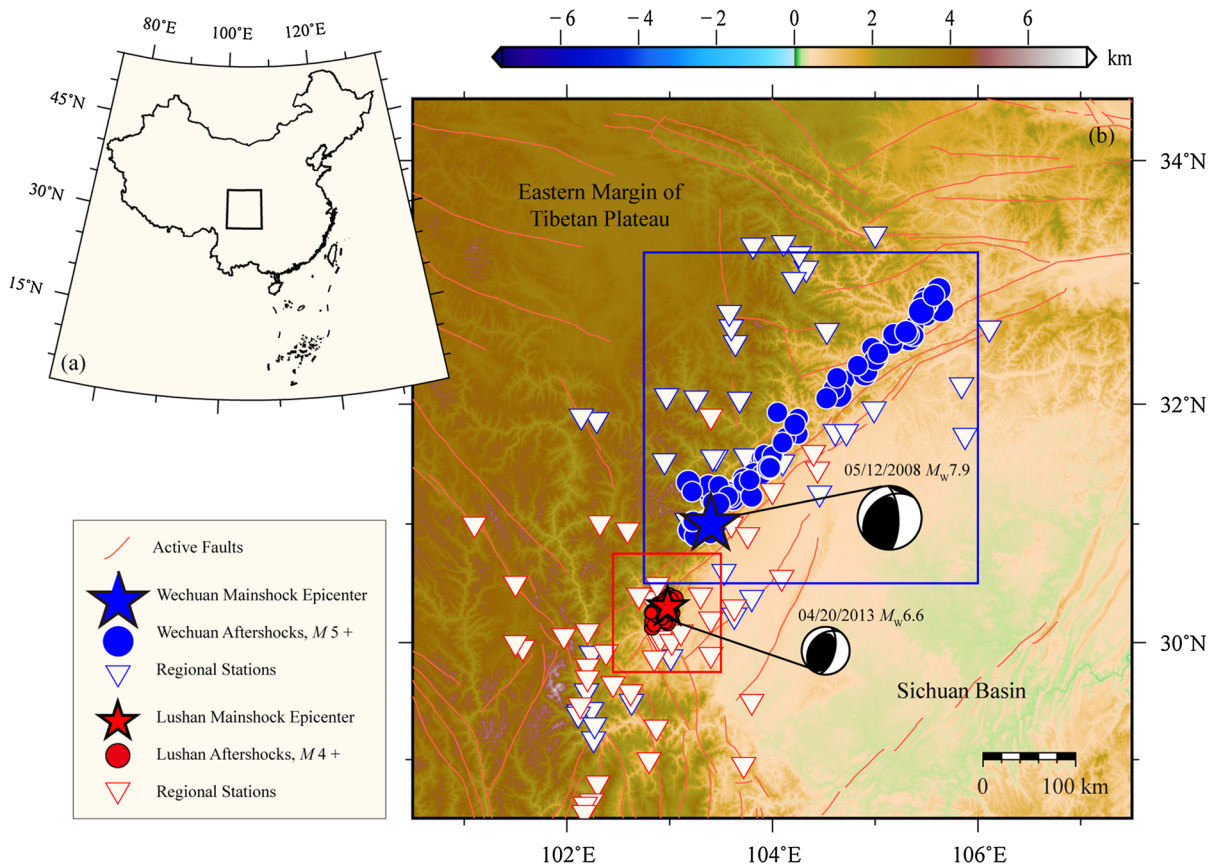


Figure 1

a Political boundary of China is shown with a black rectangle indicating the area enlarged in **b**. **b** Topographic map of Longmen Shan thrust belt with epicenters of the 2008 Wenchuan (blue star denotes the mainshock, blue circles are aftershocks) and the 2013 Lushan (red star denotes the mainshock, red circles are aftershocks) earthquake sequences obtained from China Earthquake Networks Center (CENC, see Data and Resources), and the focal mechanisms from Global Centroid Moment Tensor project (GCMT, see Data and Resources). The blue and red inverted triangles indicate the triggered strong-motion stations during the Wenchuan and Lushan mainshocks, respectively. The blue and red square delineates the areas shown in Fig. 2a, b, respectively

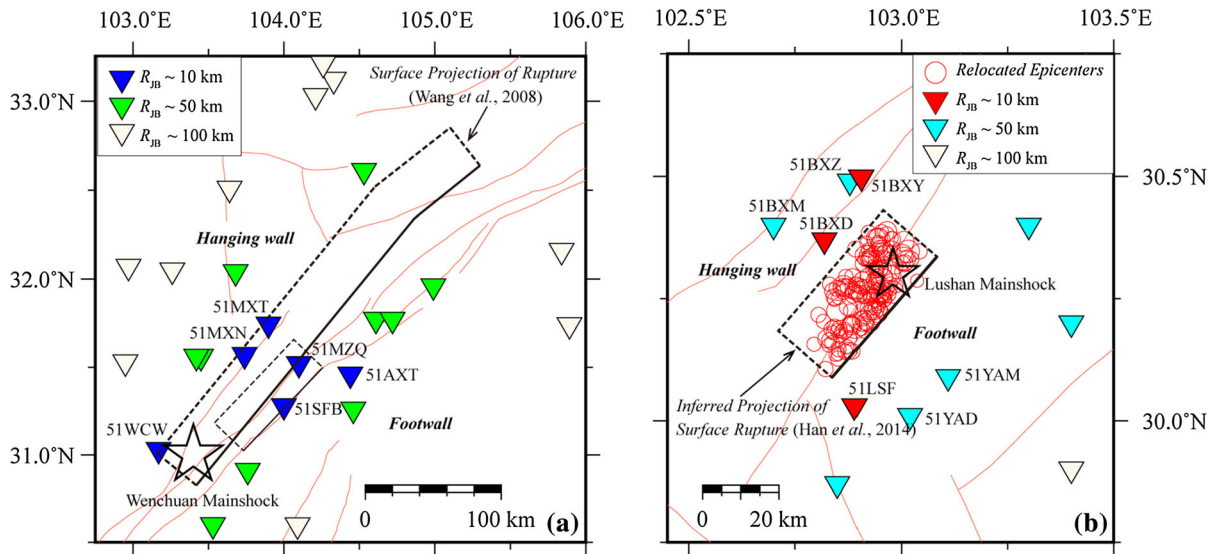


Figure 2

Finite faults (rectangles, bottom and sides of the ruptures are dashed), epicenters (stars), and triggered strong-motion stations during the Wenchuan and Lushan earthquake. Inverted triangles indicate the triggered strong-motion stations with $R_{JB} \leq 100$ km. **a** For the Wenchuan earthquake, the surface projection of rupture from Wang et al. (2008) and the 6 triggered strong-motion stations with $R_{JB} \leq 10$ km are shown as blue inverted triangles. **b** For the Lushan earthquake, the inferred surface projection of rupture based on the distribution of relocated epicenters from Han et al. (2014). The 3 triggered strong-motion stations with $R_{JB} \leq 10$ km and 4 strong-motion stations that recorded large ground motions are shown with red and blue-green inverted triangles, respectively

observed horizontal PGAs range from 40.1 to 957.7 cm/s^2 (Wang et al. 2010). There are 6 stations, 51MXT, 51MXN, 51WCW, 51MZQ, 51SFB, and 51AXT, with $R_{JB} \leq 10$ km (Fig. 2a). For the Lushan event, there are 3 and 25 stations with $R_{JB} \leq 10$ km and $R_{JB} < 100$ km, respectively (Fig. 2b). The three

near-fault stations are 51BXD, 51LSF, and 51BXY (Table 1).

2.2. Comparison of Horizontal PGAs with Ground-Motion Prediction Equations

In 2008, the Pacific Earthquake Engineering Research Center (PEER) finalized the Next Generation Attenuation (NGA-West1) project that developed a global strong-motion database involving 173 shallow crustal earthquakes in active tectonic regions (Bozorgnia et al. 2014). The NGA-West2 project updated the NGA-West1 database by adding thousands of additional ground motions recorded worldwide. The NGA-West2 database contains 21,336 components of ground-motion from 599 shallow crustal earthquakes; the magnitude measure is moment magnitude, and the two main distance measures are R_{rup} and R_{JB} . The NGA-West2 database is larger than the NGA-West1 database by about a factor of six, with moment magnitudes ranging from 3.0 to 7.9 (Ancheta et al. 2014; Bozorgnia et al. 2014; Boore et al. 2014).

Table 1

Near-fault ground motion from the Wenchuan and Lushan earthquakes

	Station name	R_{JB} (km)	Horizontal PGA (cm/s^2)	Surface rupture
Wenchuan earthquake	51MXT	0	306.6	Wang et al. (2008)
	51MXN	0	421.3	
	51WCW	0	957.7	
	51MZQ	1	824.1	
	51SFB	5	585.7	
	51AXT	10	289.5	
Lushan earthquake	51BXD	7	1005.4	Han et al. (2014)
	51LSF	10	387.4	
	51BXY	10	429.2	
	51BXZ	12	583.4	
	51BXM	18	387.2	
	51YAD	20	524.5	
	51YAM	21	400.7	

We compared horizontal components of PGA as functions of R_{JB} distance observed during the Wenchuan and Lushan mainshocks with NGA-West2. In this study, the ground-motion prediction equations (GMPE) of Boore et al. (2014; hereafter BSSA14) were used for comparison with observed horizontal PGAs. The strong-motion recordings of the 2008 Wenchuan earthquake, for instance, as one of the two largest magnitude events, with M_w 7.9, were included in the NGA-West2 database and ground-motion prediction equations. The BSSA14

model was established in the NGA-West2 project for ground-motion prediction of global shallow crustal earthquakes. Ground-motion predictions are based on the following equation (Boore et al. 2014):

$$\ln Y = F_E(\mathbf{M}, \text{mech}) + F_P(R_{JB}, \mathbf{M}, \text{region}) + F_S(V_{S30}, R_{JB}, \mathbf{M}, \text{region}, z_1) + \varepsilon_n \sigma(\mathbf{M}, R_{JB}, V_{S30}), \quad (2)$$

where $\ln Y$ represents the natural logarithm of a ground-motion parameter (i.e., PGA); F_E , F_P , and F_S represent functions for source, propagation, and site

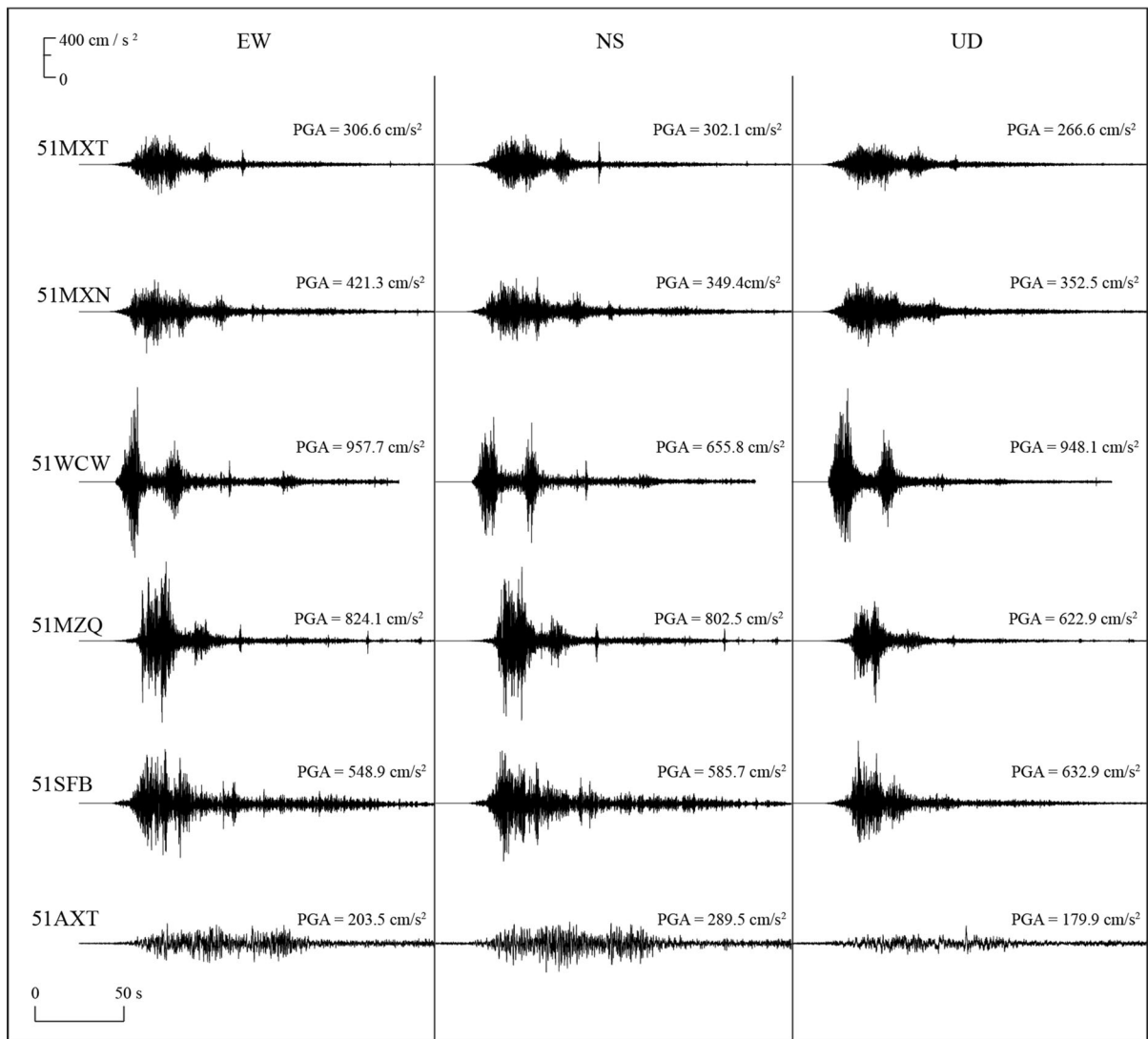


Figure 3

Acceleration time histories for NS, EW, and UD components recorded by six near-fault stations during the Wenchuan earthquake, the recorded ground motion data is provided by the CSMNC (see Data and Resources)

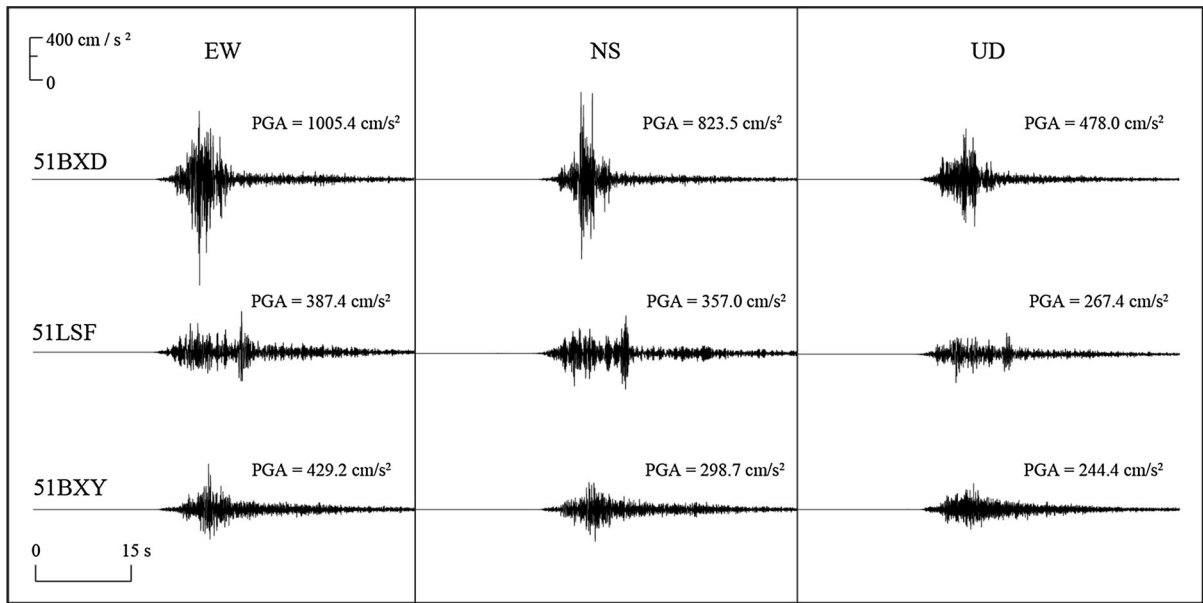


Figure 4

Acceleration time histories for EW, NS, and UD components recorded by three near-fault stations during the Lushan earthquake, the recorded ground motion data is provided by the CSMNC (see Data and Resources)

effects, respectively; ε_n is a fractional number of standard deviations of a single predicted value of $\ln Y$ away from the mean; and the σ is the total standard deviation of the model. The prediction variables are \mathbf{M} , mechanism, R_{JB} (in km), region, V_{S30} (in m/s), and depth z_1 (in km).

The shear-wave velocity averaged over the upper 30 m (V_{S30}) is commonly used to measure the site effect. V_{S30} values were not measured at stations in our study area (Wen et al. 2018), so we assumed a typical value of 350 m/s for most of the stations, which were sited on soil; the remaining data came from rock sites with assumed V_{S30} of 760 m/s (Wen and Ren 2014). Figures 5 and 6 present the comparisons between the observed horizontal PGAs from the Wenchuan and Lushan earthquakes, respectively, with GMPEs from BSSA14 (Boore et al. 2014). Near-fault observations are listed in Table 1.

Figure 5 shows that the observed PGAs from the Wenchuan earthquake are largely consistent with the predicted median values from NGA-West2 assuming $V_{S30} = 350$ m/s. Among the six near-fault stations, the horizontal PGA at the 51MXT station is sited on rock, whereas the other five stations, 51MXN, 51WCW, 51MZQ, 51SFB, and 51AXT, are on soil.

Wang et al. (2010) compared the Wenchuan data with the NGA-West1 GMPEs and pointed out that the Wenchuan data would have only a small effect in the median model predictions for the short-period ground motions in the NGA database, but the strong hanging wall effects are consistent with the NGA model at short spectral periods. For instance, the PGA at the 51WCW station on the hanging wall ($R_{JB} = 0$) is almost 30% more than the predicted median value, indicating strong hanging wall effects compared with the NGA-West2 (Fig. 5).

For the Lushan earthquake, in Fig. 6, there are three near-fault stations and four additional stations with large PGAs (Table 1); the observed PGAs at $R_{JB} < 50$ km are much higher than the predicted median values by the NGA-West2 with soil site response. The observed PGAs in the range $50 \text{ km} < R_{JB} < 200$ km are mostly higher than the GMPEs; three PGAs were significantly lower than the median on the rock. The 15 larger PGAs, more than 100 cm/s^2 , are all in the distance range $R_{JB} < 100$ km. The PGAs at the 51BXD and 51YAD stations are more than double the predicted median value; that is, NGA-West2, with $V_{S30} = 350$ m/s, under-predicted at $R_{JB} \leq 20$ km.

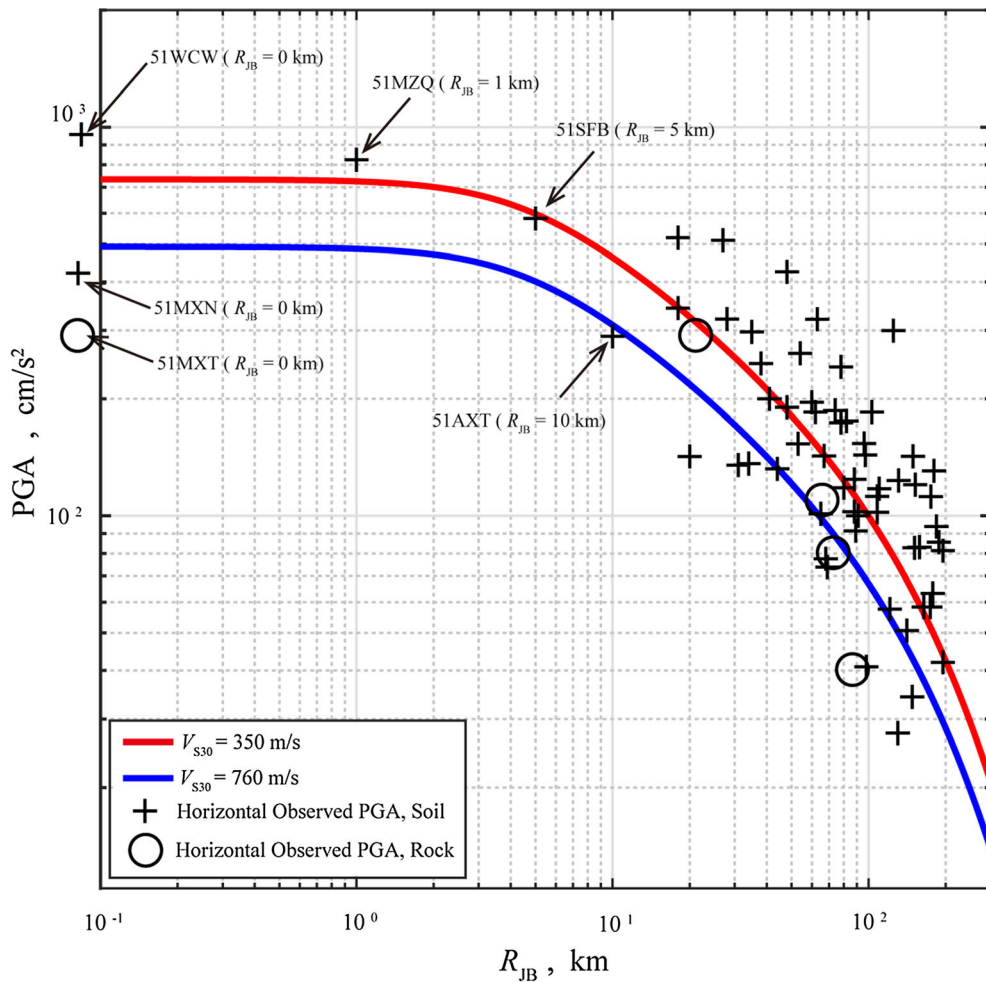


Figure 5
Comparison of the observed PGAs of the Wenchuan earthquake with NGA-West2 ($M_w = 7.9$)

The Lushan $M_w 6.6$ earthquake was well recorded by the NSMONS of China. As noted by Xie et al. (2014), the short-period ground shaking in the near-source region was strong, as evidenced by the large horizontal PGAs located within a narrow belt straddling the fault. The Lushan earthquake is a typical blind fault earthquake with large observed PGA values, but it occurred too recently for the ground motion data to be included in the NGA-West2 database. Ground motion data from the exceptionally damaging 2011 $M 6.3$ Christchurch earthquake in New Zealand, which also had no surface rupture, however, are in the NGA-West2 database. The largest PGAs for the Christchurch earthquake recorded on

the S64E, S26W, and UD components are 1163.6, 1426.7, and 1438.1 cm/s^2 , respectively, at the nearest station HVSC (Ancheta et al. 2014; Meng and Shi 2012; Meng et al. 2013).

3. Ground-Motion Simulations

In this study, the simulations of ground motion are based on a stochastic finite-fault algorithm known as EXSIM (Motazedian and Atkinson 2005; Boore 2009; Atkinson and Assatourians 2015). The stochastic method was first introduced by Hanks and McGuire (1981) and developed by Boore (1983) as a

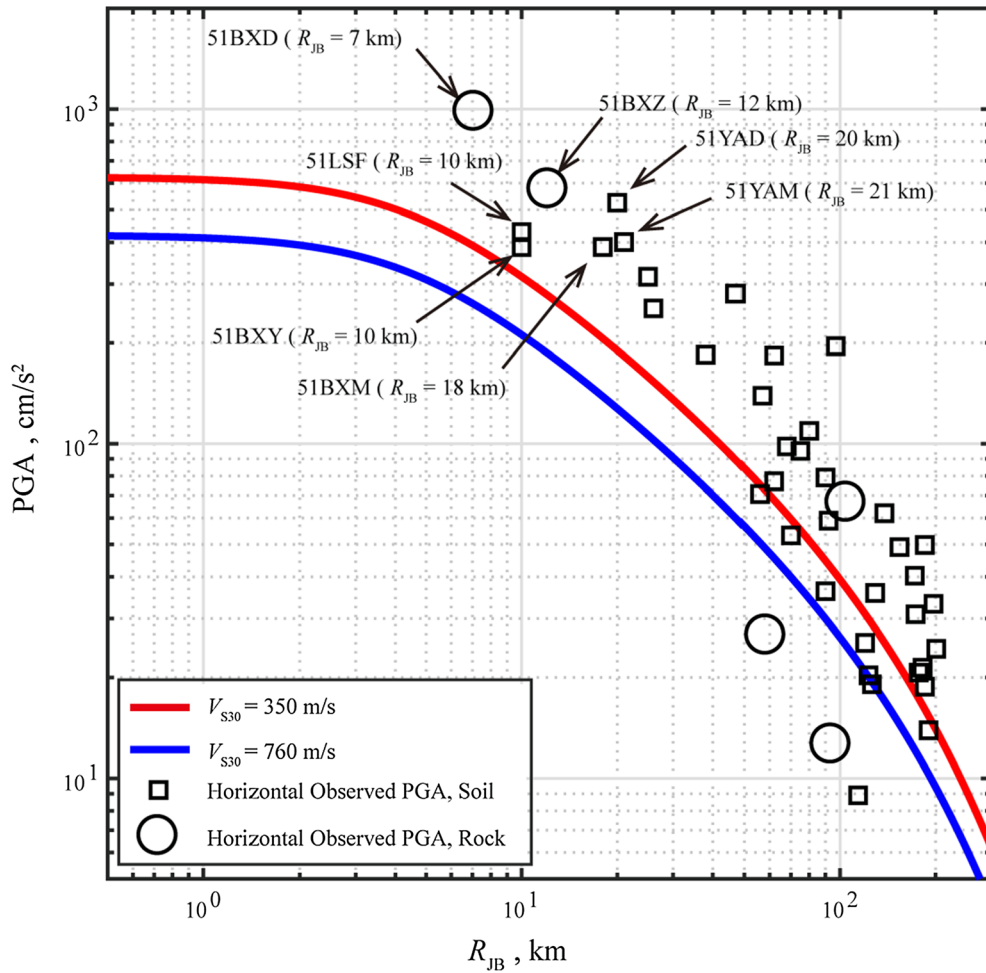


Figure 6
Comparison of the observed PGAs of the Lushan earthquake with NGA-West2 ($M_w = 6.6$)

point-source model to simulate the time series. Boore's approach is adapted for finite faults by dividing the fault into many sub-sources; the ground motion from each sub-source is expressed as random Gaussian noise of specified duration. The source spectra are then analyzed in terms of the model developed by Brune (1970, 1971). The amplitude of the spectral plateau at frequencies extending upward from the corner frequency is proportional to a stress parameter that is commonly known as the "Brune stress drop" (e.g., Hanks and McGuire 1981).

3.1. Source Parameters for the Stochastic Simulation

Simulating the ground motion of intraplate thrust earthquakes is challenging because of the complexity of their ruptures. Based on the work of Baltay et al. (2013), the following relationship can be derived between PGA and $\Delta\sigma$, the static stress drop

$$PGA = \frac{2R_{\theta\phi}(2\pi)^2\Delta\sigma}{106\rho R} \sqrt{\frac{f_{\max}}{f_c}} \sqrt{2 \ln\left(\frac{2f_{\max}}{f_c}\right)}, \quad (3)$$

where $R_{\theta\phi}$ is the radiation pattern, ρ is the density, R is the hypocentral distance, f_c is the corner frequency, and f_{\max} is the upper frequency limit of the observations.

Table 2

Input parameters applied for EXSIMs of the Wenchuan and Lushan earthquake

Wenchuan earthquake	Lushan earthquake
M_w 7.9	M_w 6.6
Sub-source size: 5 km × 5 km	Sub-source size: 2 km × 2 km
Slip model: Chen et al. (2008); Wang et al. (2008)	Slip model: Chen et al. (2013)
WC-Model-1	LS-Model-1
$\Delta\sigma = 1.5$ MPa	$\Delta\sigma = 0.85$ MPa
WC-Model-2	LS-Model-2
$\Delta\sigma = 1.9$ MPa	$\Delta\sigma \approx 2.9$ MPa
WC-Model-3	LS-Model-3
$\Delta\sigma \approx 2.0$ MPa	$\Delta\sigma \approx 3.5$ MPa
WC-Model-4	
$\Delta\sigma \approx 2.5$ MPa	
Sub-source duration (distance-dependent):	
$t = \begin{cases} 0 & R < 10 \\ 0.16 \times (R - 10) & 10\text{km} \ll R < 70\text{km} \\ 9.6 - 0.03 \times (R - 70) & 70\text{km} \ll R < 130\text{km} \\ 7.7 + 0.04 \times (R - 130) & R \gg 130\text{km} \end{cases}$	
Geometrical spreading:	
$G(R) = \begin{cases} R^{-1} & R < 70\text{km} \\ 1/70 & 70\text{km} \ll R \ll 130\text{km} \\ R^{-0.5} & R \gg 130\text{km} \end{cases}$	
^a Anelastic attenuation: $Q(f) = 274.6 f^{0.423}$	
Kappa: 0.05 s	
Shear-wave velocity: $\beta = 3.7$ km/s	
Rupture velocity: $v_R = 3.0$ km/s	
Density: 2.8 g/cm ³	

Some input parameters are the same as in Meng and Shi (2011), Meng et al. (2014)

^aQuality factor is from Hua et al. (2009)

Following Hanks and McGuire (1981), we have analyzed PGAs using stochastic simulations of ground acceleration at six near-fault stations near the Wenchuan earthquake and seven near the Lushan earthquake (Table 1). Table 2 lists input parameters for simulating synthetic acceleration time series; the main inputs are the source parameters, fault geometry, and anelastic attenuation. In EXSIM, all sub-sources are assumed to have the same stress drop, which is perhaps the most important factor controlling high-frequency ground motion. The models calculated here and their stress drops are listed in Table 2.

3.2. EXSIM Results for the Wenchuan earthquake

In Fig. 7, we see a comparison of synthetic horizontal acceleration time series of the Wenchuan earthquake with observations at six near-fault

stations. The whole waveform trace lasted more than 100 s, and in most cases, the envelope and duration of synthetic ground motions matched, at least roughly, the observed waveforms. We also see that the simulated PGAs varied with different assumed stress drops. The synthetic acceleration time histories from three hanging-wall stations, 51MXT, 51MXN, and 51WCW, are all located in the surface projected rupture area (Fig. 2). Compared with the observations, the simulated PGAs with various stress drops at the stations 51MXT and 51MXN matched better than the simulations at station 51WCW.

Station 51MZQ is much closer to both epicenters and the largest asperity of the main fault plane (Chen et al. 2008; Wang et al. 2008), whereas the simulated PGA at this station by the WC-Model-4 is much higher than the observations. Simulated PGAs at station 51SFB are lower than observations there; however, the predicted median values from BSSA14

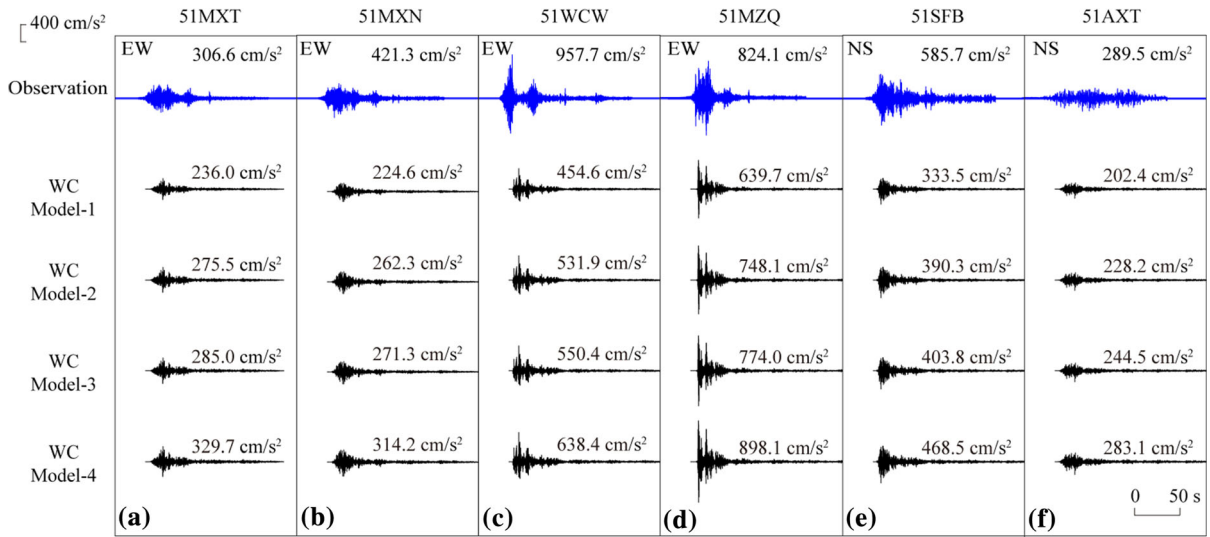


Figure 7

Comparisons of the observed (blue) and synthetic (black) horizontal acceleration time series at six near-fault stations (see Table 1) for the Wenchuan earthquake

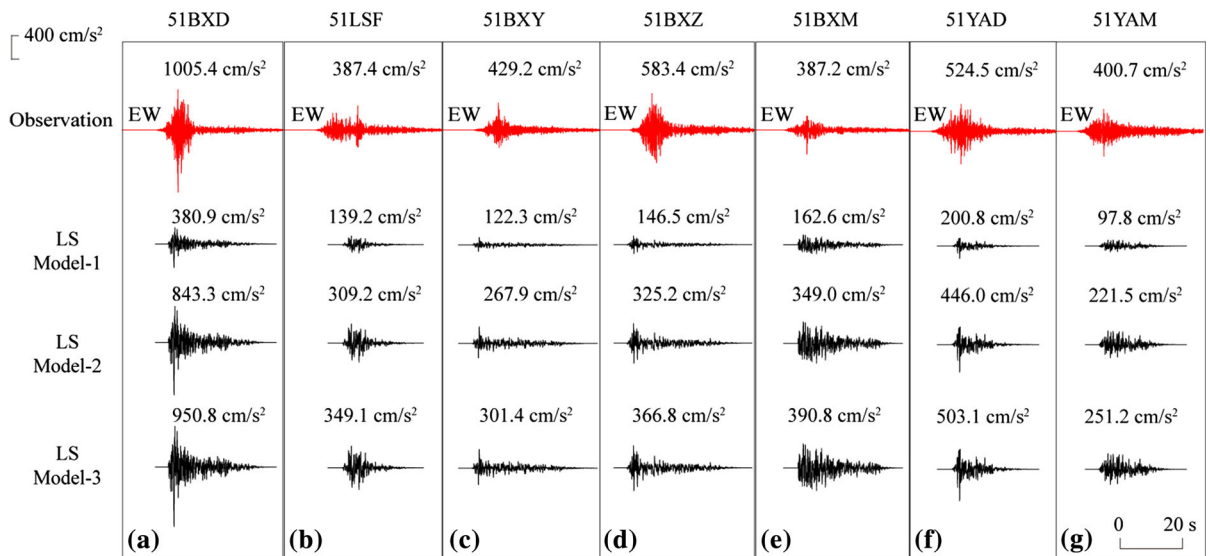


Figure 8

Comparisons of the observed (red) and synthetic (black) horizontal acceleration time series at three near-fault stations and four additional stations (see Table 1) for the Lushan earthquake

with the same V_{S30} value is much more consistent with the observations at the same station (Fig. 5). We also note that the best choice of stress drop, based on the results in Fig. 7, is about 2.5 MPa (model 4).

3.3. EXSIM Results for the Lushan Earthquake

In Fig. 8, we compared synthetic horizontal acceleration time series of the Lushan earthquake with observations at three near-fault stations and an additional four stations with large PGAs (Table 1).

We simulated the synthetic acceleration time series from four hanging-wall stations and three footwall stations, respectively (Fig. 2b). The whole waveform trace lasted more than 40 s, and in most cases, the envelope and duration of synthetic ground motions also matched the observed waveform, at least approximately.

As noted earlier, the apparent stress for the Lushan earthquake is about 0.75 MPa. The simulated PGAs from the Lushan-Model-3 with a stress drop of 3.5 MPa matched the observed PGAs better than those from the other two models. For the Lushan earthquake, the ratio of inferred stress drop to apparent stress is about 5, which is consistent with Eq. (3) and the ratio of “Brune stress drop” to apparent stress in the Brune source model (Brune 1970, 1971).

As seen in Fig. 8 and Table 2, the simulated PGAs based on model 3 at stations 51BXD and 51BXM are consistent with the observed values. However, the simulated PGAs at stations 51BXY and 51BXZ are obviously smaller, even with the high stress drop value in model 3. The simulated PGAs based on model 3 at stations 51LSF and 51YAD are reasonably similar to the observed ground motions, whereas the simulated PGA at station 51YAM is smaller than its observed counterpart. Comparing the simulated results from stations 51YAD and 51YAM, located in the Sichuan Basin at comparable epicentral distance and R_{JB} , the differences in PGAs may perhaps be due to differences in site amplification.

4. Discussion and Conclusions

We used the GMPE for PGA from NGA-West2 to compare the observations of high-frequency ground motion from the Wenchuan and Lushan earthquakes and found that the PGAs from the Lushan event are somewhat higher than predicted by the NGA-West2 model, whereas those for the Wenchuan earthquake are in reasonably good agreement. The observed PGAs for the Wenchuan earthquake, with $R_{JB} > 20$ km, matched the GMPE with the $V_{S30} = 350$ m/s. For the Lushan earthquake, observations at distances up to 50 km are systematically larger than the median values from NGA-West2.

The stress changes associated with fault slip, as measured by either the static stress drop or the apparent stress, appear to be the important factors controlling the PGAs. Other aspects of the earthquake rupture, such as seismic moment, whether the rupture extends to the surface, and directivity seem to be of little consequence in controlling PGA, a result that is consistent with those found in investigations of many other earthquakes (e.g., Hanks and McGuire 1981).

5. Data and Resources

Data for this study are provided by China Strong Motion Network Centre (CSMNC) at <http://www.csmnc.net> (last accessed May 2013), Institute of Engineering Mechanics, China Earthquake Administration. The earthquake catalog is obtained from the China Earthquake Datacenter at <http://data.earthquake.cn/> (last accessed June 2018). The seismic moment for the Wenchuan and Lushan earthquakes used in source parameter calculation was obtained from the Global Centroid Moment Tensor catalog at <http://www.globalcmt.org> (last accessed July 2018). The radiated energy results for the Wenchuan and Lushan earthquakes were obtained from the “Energy and Broadband Solution” from United States Geological Survey at <https://earthquake.usgs.gov/earthquakes/> (last accessed May 2013). GMT is available at <http://www.soest.hawaii.edu/gmt> (last accessed May 2018).

Acknowledgements

This study is supported by the National Natural Science Foundation of China (41404045, 41504047), the National Key R & D Program of China (2017YFC1500502), and China Scholarship Council (no. 201704190041). We thank Jon B. Fletcher, Walter D. Mooney, and Elizabeth S. Cochran of the United States Geological Survey for their insightful reviews that improved this manuscript. We are grateful Han Libo providing the relocated catalog of the Lushan earthquake.

Publisher's Note Springer Nature remains neutral with regard to jurisdictional claims in published maps and institutional affiliations.

REFERENCES

- Ancheta, T. D., Darragh, R. B., Stewart, J. P., Seyhan, E., Silva, W. J., Chiou, B. S. J., et al. (2014). NGA-West2 database. *Earthquake Spectra*, 30(3), 989–1005.
- Atkinson, G. M., & Assatourians, K. (2015). Implementation and validation of EXSIM (a stochastic finite-fault ground-motion simulation algorithm) on the SCEC broadband platform. *Seismological Research Letters*, 86(1), 48–60.
- Baltay, A. S., Hanks, T. C., & Beroza, G. C. (2013). Stable stress-drop measurements and their variability: Implications for ground—motion prediction. *Bulletin of the Seismological Society of America*, 103(1), 211–222.
- Boore, D. M. (1983). Stochastic simulation of high-frequency ground motions based on seismological models of the radiated spectra. *Bulletin of the Seismological Society of America*, 73(6A), 1865–1894.
- Boore, D. M. (2009). Comparing stochastic point-source and finite-source ground-motion simulations: SMSIM and EXSIM. *Bulletin of the Seismological Society of America*, 99(6), 3202–3216.
- Boore, D. M., Stewart, J. P., Seyhan, E., & Atkinson, G. M. (2014). NGA-West2 equations for predicting PGA, PGV, and 5% damped PSA for shallow crustal earthquakes. *Earthquake Spectra*, 30(3), 1057–1085.
- Bozorgnia, Y., Abrahamson, N. A., Atik, L. A., Ancheta, T. D., Atkinson, G. M., Baker, J. W., et al. (2014). NGA-West2 research project. *Earthquake Spectra*, 30(3), 973–987.
- Brune, J. N. (1970). Tectonic stress and the spectra of seismic shear waves from earthquakes. *Journal of Geophysical Research*, 75(26), 4997–5009.
- Brune, J. N. (1971). Tectonic stress and the spectra of seismic shear waves from earthquakes: Correction. *Journal of Geophysical Research*, 76, 5002.
- Chen, Y. T., Xu, L. S., Zhang, Y., Du, H. L., Feng, W. P., Liu, C., & Li, C. L. (2008). Analysis of the source characteristics of the great wenchuan earthquake of May 12, 2008 (in Chinese). <https://wenku.baidu.com/view/2daab817866fb84ae45c8dda.html>. Accessed May 2013
- Chen, Y. T., Yang, Z. X., Zhang, Y., & Liu, C. (2013). From 2008 Wenchuan earthquake to 2013 Lushan earthquake. *Scientia Sinica Terrae*, 43(6), 1064–1072. (In Chinese).
- Han, L., Zeng, X., Jiang, C., Ni, S., Zhang, H., & Long, F. (2014). Focal mechanisms of the 2013 M_W 6.6 Lushan, China earthquake and high-resolution aftershock relocations. *Seismological Research Letters*, 85(1), 8–14.
- Hanks, T. C., & McGuire, R. K. (1981). The character of high-frequency strong ground motion. *Bulletin of the Seismological Society of America*, 71(6), 2071–2095.
- Hua, W., Chen, Z. L., & Zheng, S. H. (2009). A study on segmentation characteristics of aftershock source parameters of the Wenchuan $M8.0$ Earthquake in 2008. *Chinese Journal of Geophysics*, 52(1), 130–137. (In Chinese with English abstract).
- Li, X., Zhou, Z., Huang, M., Wen, R., Yu, H., Lu, D., et al. (2008). Preliminary analysis of strong-motion recordings from the magnitude 8.0 Wenchuan, China, earthquake of 12 May 2008. *Seismological Research Letters*, 79(6), 844–854.
- Meng, L., & Shi, B. (2011). Near-fault strong ground motion simulation of the May 12, 2008, M_W 7.9 Wenchuan earthquake by dynamical composite source model. *Chinese Journal of Geophysics*, 54(4), 1010–1027. (In Chinese with English abstract).
- Meng, L., & Shi, B. (2012). Source rupture process of the February 21, 2011, M_W 6.1, New Zealand earthquake and the characteristics of the near-field strong ground motion. *Chinese Journal of Geophysics*, 55(5), 632–641.
- Meng, L., Shi, B., & Liu, J. (2013). Characteristics of strong ground motion from the sequence of New Zealand earthquake: 2010, M_W , 7.0, main shock and 2011, M_W , 6.1, aftershock. *Acta Seismologica Sinica*, 35(3), 351–368. (In Chinese with English abstract).
- Meng, L., Zhou, L., & Liu, J. (2014). Estimation of the near-fault strong ground motion and intensity distribution of the 2013 Lushan, Sichuan, M_S 7.0 earthquake. *Chinese Journal of Geophysics*, 57(2), 441–448. (In Chinese with English abstract).
- Mooney, W. D., & Wang, H. (2014). Seismic intensities, PGA, and PGV for the 20 April 2013, M w 6.6 Lushan, China, earthquake, and a comparison with North America. *Seismological Research Letters*, 85(5), 1034–1042.
- Motazedian, D., & Atkinson, G. M. (2005). Stochastic finite-fault modeling based on a dynamic corner frequency. *Bulletin of the Seismological Society of America*, 95(3), 995–1010.
- Ren, Y., Wang, H., Xu, P., Dhakal, Y. P., Wen, R., Ma, Q., et al. (2018). Strong-motion observations of the 2017 M_S 7.0 Jiuzhaigou earthquake: comparison with the 2013 M_S 7.0 Lushan earthquake. *Seismological Research Letters*, 89(4), 1354–1365.
- Wang, C. Y., Han, W. B., Wu, J. P., Lou, H., & Chan, W. W. (2007). Crustal structure beneath the eastern margin of the Tibetan Plateau and its tectonic implications. *Journal of Geophysical Research: Solid Earth*. <https://doi.org/10.1029/2005JB003873>.
- Wang, Z., & Lu, M. (2011). A short note on ground-motion recordings from the M 7.9 Wenchuan, China, earthquake and ground-motion prediction equations in the Central and Eastern United States. *Seismological Research Letters*, 82(5), 731–734.
- Wang, H., Ren, Y., & Wen, R. (2018). Source parameters, path attenuation and site effects from strong-motion recordings of the Wenchuan aftershocks (2008–2013) using a non-parametric generalized inversion technique. *Geophysical Journal International*, 212(2), 872–890.
- Wang, D., Xie, L., Abrahamson, N. A., & Li, S. (2010). Comparison of strong ground motion from the Wenchuan, China, earthquake of 12 May 2008 with the Next Generation Attenuation (NGA) ground-motion models. *Bulletin of the Seismological Society of America*, 100(5B), 2381–2395.
- Wang, W., Zhao, L., Li, J., & Yao, Z. X. (2008). Rupture process of the M_S 8.0 Wenchuan earthquake of Sichuan, China. *Chinese Journal of Geophysics*, 51(5), 1403–1410. (In Chinese with English abstract).
- Wen, R., & Ren, Y. (2014). Strong-motion observations of the Lushan earthquake on 20 April 2013. *Seismological Research Letters*, 85(5), 1043–1055.
- Wen, R., Xu, P., Wang, H., & Ren, Y. (2018). Single-station standard deviation using strong-motion data from sichuan region, China. *Bulletin of the Seismological Society of America*, 108(4), 2237–2247.

- Wyss, M., & Brune, J. N. (1968). Seismic moment, stress, and source dimensions for earthquakes in the California-Nevada region. *Journal Geophysical Research*, 73(14), 4681–4694.
- Xie, J., Li, X., Wen, Z., & Wu, C. (2014). Near-source vertical and horizontal strong ground motion from the 20 April 2013 Mw 6.8 Lushan earthquake in China. *Seismological Research Letters*, 85(1), 23–33.
- Xu, X., Wen, X., Han, Z., Chen, G., Li, C., Zheng, W., et al. (2013). Lushan M_S 7.0 earthquake: A blind reverse-fault earthquake. *Chinese Science Bulletin*, 58(28–29), 3437–3443.
- Xu, X., Wen, X., Yu, G., Chen, G., Klinger, Y., Hubbard, J., et al. (2009). Coseismic reverse-and oblique-slip surface faulting generated by the 2008 M_W 7.9 Wenchuan earthquake. *China Geology*, 37(6), 515–518.
- Zhang, Z., Wang, W., Ren, Z., Zhang, P., Fang, L., & Wu, J. (2013). Lushan M_S 7.0 earthquake: A special earthquake occurs on curved fault. *Chinese Science Bulletin*, 58(28–29), 3483–3490.

(Received September 6, 2018, revised July 12, 2019, accepted July 29, 2019, Published online August 8, 2019)